

# Effective destruction of CO by cosmic rays: implications for tracing H<sub>2</sub> gas in the Universe

Thomas G. Bisbas

*Department of Physics and Astronomy, University College London, Kathleen Lonsdale Building, Gower Place, WC1E 6BT, London*

t.bisbas@ucl.ac.uk

Padelis P. Papadopoulos

*School of Physics and Astronomy, Cardiff University, Queen's Buildings, The Parade, Cardiff, CF24 3AA, UK*

*Research Center for Astronomy, Academy of Athens, Soranou Efessiou 4, GR-115 27 Athens, Greece*

and

Serena Viti

*Department of Physics and Astronomy, University College London, Kathleen Lonsdale Building, Gower Place, WC1E 6BT, London*

## ABSTRACT

We report on the effects of cosmic rays (CRs) on the abundance of CO in H<sub>2</sub> clouds under conditions typical for star-forming galaxies in the Universe. We discover that this most important molecule for tracing H<sub>2</sub> gas is very effectively destroyed in ISM environments with CR energy densities  $U_{\text{CR}} \sim (50 - 10^3) \times U_{\text{CR,Gal}}$ , a range expected in numerous star-forming systems throughout the Universe. This density-dependent effect operates volumetrically rather than only on molecular cloud surfaces (i.e. unlike FUV radiation that also destroys CO), and is facilitated by: a) the direct destruction of CO by CRs, and b) a reaction channel activated by CR-produced He<sup>+</sup>. The effect we uncover is strong enough to render Milky-Way type Giant Molecular Clouds (GMCs) very CO-poor (and thus CO-untraceable), even in ISM environments with rather modestly enhanced average CR energy densities of  $U_{\text{CR}} \sim (10 - 50) \times U_{\text{CR,Gal}}$ . We conclude that the CR-induced destruction of CO in molecular clouds, unhindered by dust absorption, is perhaps the single most important factor controlling the CO-visibility of

molecular gas in vigorously star-forming galaxies. We anticipate that a second order effect of this CO destruction mechanism will be to make the H<sub>2</sub> distribution in the gas-rich disks of such galaxies appear much clumpier in CO  $J=1-0$ ,  $2-1$  line emission than it actually is. Finally we give an analytical approximation of the CO/H<sub>2</sub> abundance ratio as a function of gas density and CR energy density for use in galaxy-size or cosmological hydrodynamical simulations, and propose some key observational tests.

*Subject headings:* (ISM:) cosmic rays – astrochemistry – methods: numerical – ISM: abundances – (ISM:) photon-dominated region (PDR) – galaxies: ISM

## 1. Introduction

Using the mm/submm rotational transitions of CO, the most abundant molecule after H<sub>2</sub> (CO/H<sub>2</sub>  $\sim 10^{-4}$ ), as tracers of the H<sub>2</sub> distribution and average physical conditions in galaxies is now a well-established method, and indeed a main driver behind the largest ground-based astronomical facility on Earth, the Atacama Large Millimeter Array (ALMA) in Llano Chajnantor of North Chile. Ever since the first detection of a bright CO  $J = 1 - 0$  line in Orion (Wilson et al. 1970) there has been tremendous progress towards detecting ever higher- $J$  transitions of CO, in our own Galaxy as well as in others (e.g. Cronin et al. 1976; Guesten et al. 1993; Devereux et al. 1994; Dumke et al. 2001; Yao et al. 2003a,b; Mao et al. 2010; Papadopoulos et al. 2007; Papadopoulos 2010; Leech et al. 2010) and of other molecules such as HCN, HCO<sup>+</sup>, and CS (Nguyen et al. 1992; Solomon et al. 1992; Paglione et al. 1997; Gao & Solomon 2004; Graciá-Carpio et al. 2006, 2008; Papadopoulos 2007; Krips et al. 2008; Greve et al. 2009; Zhang et al. 2014). The relative strengths of such lines can then be used as powerful probes of the average density, temperature, and dynamical state (i.e. gravitationally bound or unbound) of the molecular gas in galaxies (Papadopoulos et al. 2012, and references therein). A lot of effort has been focused particularly towards using the two lowest CO rotational lines as H<sub>2</sub> gas mass tracers in galaxies via the so-called  $X_{\text{CO}}$ -factor (e.g. Dickman et al. 1986; Maloney & Black 1988; Young & Scoville 1991; Solomon et al. 1992; Bryant & Scoville 1996; Solomon et al. 1997; Downes & Solomon 1998). In this context higher- $J$  CO and other molecular lines remain very important since the constraints they set on the average density, thermal and dynamical state of H<sub>2</sub> cloud ensembles<sup>1</sup> help determine  $X_{\text{CO}}$  and find whether it deviates from its Galactic calibrated value  $X_{\text{CO,Gal}} \sim 5 X_{\ell}^2$  (see

---

<sup>1</sup> $X_{\text{CO}}$  retains its mass-tracing value only for cloud ensembles rather than cloud parts or single H<sub>2</sub> clouds

<sup>2</sup> $X_{\ell} = M_{\odot}(\text{K km s}^{-1} \text{ pc}^2)^{-1}$

Papadopoulos et al. 2012, for a recent such study).

Nevertheless, all available studies quantifying the effects of the  $\text{H}_2$  physical conditions on the  $(\text{H}_2 \text{ mass})/(\text{CO luminosity})$  ratio rely on the premise of a CO-rich  $\text{H}_2$  gas phase. Significantly lower CO/ $\text{H}_2$  ratios would render the use of CO lines as molecular gas mass tracers problematic. Extensive observational and theoretical work has indeed shown that a CO-poor phase becomes possible for ISM with low average metallicities ( $Z \lesssim 0.2Z_\odot$ ) and strong FUV fields (e.g. Maloney & Black 1988; Madden et al. 1997; Israel 1997; Pak et al. 1998; Bell et al. 2006a). Metallicity ( $Z$ ) and the average FUV radiation field ( $G_\odot$ ) then emerge as the two most important factors determining CO/ $\text{H}_2$  in metal-poor ISM, while models that incorporate the underlying ISM physics have been made to correct for such CO-dark  $\text{H}_2$  mass per cloud (Pak et al. 1998; Bolatto et al. 1999). These can be of help as long as: a) some CO survives in the inner cloud regions (so that CO line emission can still mark such clouds), b) the average metallicity and mean FUV radiation field are known (so that their values can be inserted in the models). Such models will obviously not work for metallicities that fall too low and/or average FUV fields that are strong enough to keep CO fully dissociated<sup>3</sup> (e.g. Bolatto et al. 1999; Bell et al. 2006b).

Despite existing theoretical work that investigated the effects of CRs on ISM chemistry (e.g. Bayet et al. 2011; Meijerink et al. 2011), the effects on CO/ $\text{H}_2$  of CRs (which, unlike FUV radiation, travel nearly unimpeded through the irrespective of its dust content), or their impact on the observability of  $\text{H}_2$  gas via CO lines has not been investigated in detail. Recently, Bialy & Sternberg (2014) presented an analytical study of the importance of CRs in the abundance of the most important species under different metallicities, using isothermal calculations. In this work, we present our investigation of the effects produced by CRs starting with the ISM of metal-rich star-forming galaxies but, unlike Bialy & Sternberg (2014), we perform full thermochemical calculations (i.e. we solve for thermal balance) while using a much more extensive chemical network. We assume CRs fully penetrating the molecular clouds, with an average CR energy density scaling as  $U_{\text{CR}} \propto \rho_{\text{SFR}}$  (where  $\rho_{\text{SFR}}$  is the average star-formation rate energy density; see Papadopoulos 2010, and references therein for detailed arguments).

---

<sup>3</sup>For clarity we must emphasize here that even in the CO-rich parts of the Galaxy CO-poor regions do exist (e.g. diffuse  $\text{H}_2$  clouds, outer parts of GMCs, regions very near O, B stars), but their masses are typically too small to make any impact on the total  $\text{H}_2$  mass budget as traced by the CO-rich  $\text{H}_2$  gas.

## 2. The effect of CRs on the CO/H<sub>2</sub> ratio in molecular clouds

We first perform a grid of runs of one-dimensional uniform density clouds in which we vary the density,  $n_{\text{H}}$ , from  $(10^2 - 10^5) \text{ cm}^{-3}$  and the cosmic ray ionization rate,  $\zeta_{\text{CR}}$ , from  $10^{-17} - 10^{-13} \text{ s}^{-1}$ . The choice for the  $\zeta_{\text{CR}}$  range is dictated by that deduced within the Milky Way ( $\sim (1 - 5) \times 10^{-17} \text{ s}^{-1}$ ), and from the  $\zeta_{\text{CR}}$  expected in galaxies with star-formation (SF) rate densities of  $\rho_{\text{SFR}} \sim (1 - 10^3) \times \rho_{\text{SFR, Gal}}$  (assuming  $\zeta_{\text{CR}} \propto U_{\text{CR}}$  where  $U_{\text{CR}}$  is the CR energy density, and  $U_{\text{CR}} \propto \rho_{\text{SFR}}$  for a CR-transparent ISM).

In order to isolate the effects of CRs on the important CO/H<sub>2</sub> ratio we set the incident FUV field  $G = 0G_{\odot}$  ( $G_{\odot}$  the average interstellar radiation field as described by Draine 1978), and consider only Solar metallicity ( $Z=Z_{\odot}$ ) gas. We chose a density range that encompasses the low-density Galactic regions where the HI→H<sub>2</sub> phase transition takes place in the Cold Neutral Medium ( $\langle n_{\text{H}} \rangle \sim 200 \text{ cm}^{-3}$ ), to typical Galactic GMCs ( $\langle n_{\text{H}} \rangle \sim 500 - 10^3 \text{ cm}^{-3}$ ), and up to the high densities typical of SF cores ( $\langle n_{\text{H}} \rangle \sim 10^5 \text{ cm}^{-3}$ ). We then use the 3D-PDR code (see Appendix A) to conduct full thermochemical calculations on a uniform density cloud permeated by an average  $U_{\text{CR}}$  (that proportionally sets  $\zeta_{\text{CR}}$ ) for the grid of  $[n_{\text{H}} - \zeta_{\text{CR}}]$  values. The results on the CO/H<sub>2</sub> ratio (blue lines, marking CO/H<sub>2</sub> =  $10^{-5}$ ) can be viewed in Fig. 1, where we also show the C I/CO ratio (green lines, indicating the C I/CO= 5 ratio) since atomic carbon is the dominant species resulting from the CR-induced destruction of CO.

From Fig.1 it can be seen that molecular clouds with densities typical of the Galactic GMC density range ( $\sim 10^2 - 10^3 \text{ cm}^{-3}$ ) can become very CO-poor even in ISM environments with SFR densities (and thus  $U_{\text{CR}}$ ) only  $\sim 10 \times$  Galactic. This is even more the case for the ISM of gas-rich SF systems like the so-called BzK galaxies. These are isolated disks, typically at  $z \sim 1 - 2$ , with SFR  $\sim (50 - 150) \times$  Galactic, and representative of a major SF mode in the Early Universe (Daddi et al. 2010). In such systems CO/H<sub>2</sub>  $< 10^{-5}$  (10 times less abundant than in the Galaxy) *for much of the range of average H<sub>2</sub> gas densities typical for Galactic GMCs*. Thus, unless the molecular gas in such galaxies lies preferentially in cloud structures with  $n(\text{H}_2) > 10^3 \text{ cm}^{-3}$ , CO imaging for the purpose of revealing H<sub>2</sub> gas disk sizes, average molecular gas physical conditions, and H<sub>2</sub> mass distribution (e.g. Daddi et al. 2010, 2014) may be inadequate. Figure 1 also reveals that efficient CR-induced CO destruction encompasses ever increasing gas densities for higher  $\zeta_{\text{CR}}$ , reaching up to  $n \sim 10^4 \text{ cm}^{-3}$  for  $\zeta_{\text{CR}}$  values expected in compact merger/starburst galaxies in the local Universe (ULIRGs), and similar systems like the so-called Submm Galaxies (SMGs) found at much larger numbers in the distant Universe (Smail et al. 1997; Hughes et al. 1998)

Furthermore, even in the Galaxy there seems to be a  $[n_{\text{H}} - \zeta_{\text{CR}}]$  parameter space where low-density molecular gas ( $n_{\text{H}} \sim (1 - 3) \times 10^2 \text{ cm}^{-3}$ ) can be very CO-poor. Such a gas phase may indeed exist in the outer Galactic disk ( $R_{\text{Gal}} \geq 15 \text{ kpc}$ ) where a combination of

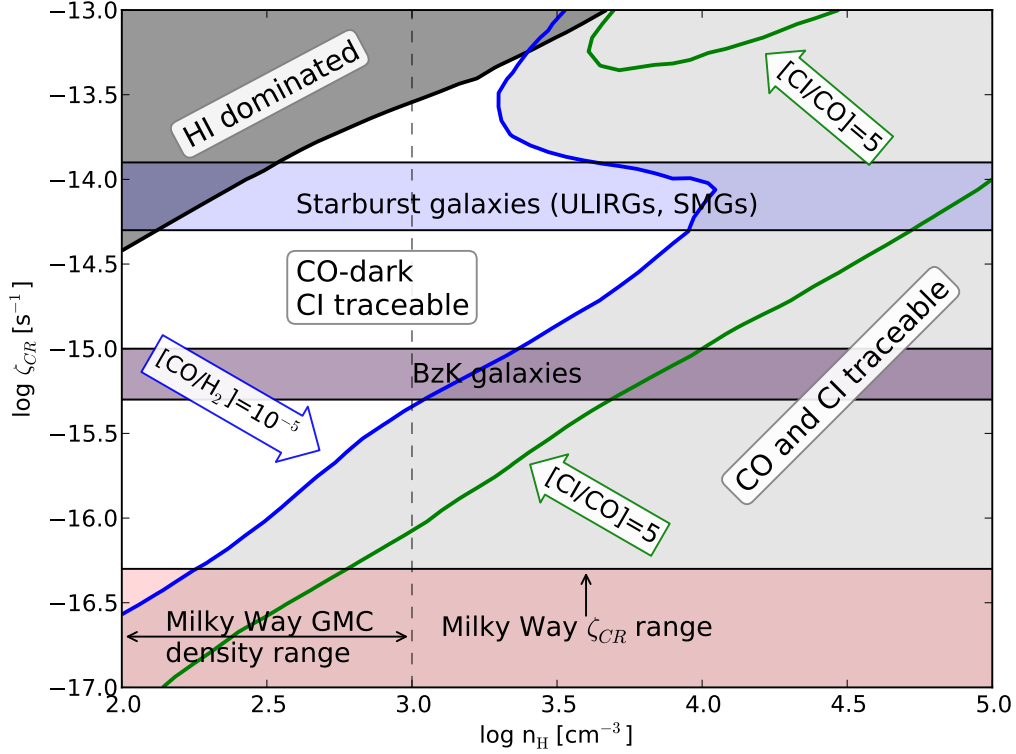


Fig. 1.— Map showing the traceability of  $\text{H}_2$  using CO and CI as a function of H number density  $n_{\text{H}}$  and the cosmic-ray ionization rate  $\zeta_{\text{CR}}$ . The three horizontal areas correspond to the  $\zeta_{\text{CR}}$  range for (from bottom to top) the Milky Way, BzK galaxies, and Starburst galaxies. The shaded area below the blue line ( $\text{CO}/\text{H}_2 = 10^{-5}$ ) corresponds to the region for which CO and CI can both trace  $\text{H}_2$ . The region above the blue line and below the top left dark-shaded region corresponds to the area in which CO has been destroyed by cosmic-rays but  $\text{H}_2$  survives, making CI the only possible tracer. The dark-shaded region on top left corresponds to the area where  $\text{H}_2$  is also destroyed by the interaction of cosmic rays hence being rich in HI ( $\text{HI}/2\text{H}_2 = 1$ ). Note that for  $\zeta_{\text{CR}} > 10^{-14} \text{ s}^{-1}$  CO is destroyed less effectively for lower densities than  $n_{\text{H}} = 10^4 \text{ cm}^{-3}$  due to the destruction of  $\text{He}^+$ . In §4.1 we discuss the chemistry behind this behaviour.

low metallicities ( $Z \sim 0.15 - 0.2Z_{\odot}$ ) and low densities keep CO formation rates low while a still substantial FUV radiation field maintains high CO destruction rates. This can yield a CO-dark  $\text{H}_2$  phase that can be quite massive (Papadopoulos et al. 2002). Any additional CO destruction due to CRs (which propagate freely to the outer Galactic disk) can only further reduce CO/ $\text{H}_2$ , rendering the corresponding molecular gas phase even harder to detect via CO line emission (see also Wolfire et al. 2010, for a recent study of CO-dark  $\text{H}_2$  gas in the Galaxy).

### 2.1. The intensity of CO $J=1-0$ , $2-1$ and CI $1-0$ , $2-1$ lines

We will now examine the emergent intensities of the CO  $J=1-0$ ,  $2-1$  ( $\sim 115$  GHz,  $\sim 230$  GHz) and CI  $J=1-0$ ,  $2-1$  ( $\sim 492$  GHz,  $\sim 809$  GHz) lines across the  $[\text{n}_{\text{H}} - \zeta_{\text{CR}}]$  parameter space shown in Fig. 1, in order to access their detectability in CO-poor versus CO-rich gas phases. We choose only the two lowest- $J$  CO lines as the only CO transitions that are not excitation-biased, when it comes to the underlying state of the gas necessary to significantly excite them. Higher- $J$  CO lines will trace mainly warm and dense  $\text{H}_2$  gas ( $n \gtrsim 10^4 \text{ cm}^{-3}$ ,  $E_{\text{J}}/k_{\text{B}} \gtrsim 30 \text{ K}$ ), and are not reliable tracers of the general  $\text{H}_2$  gas distribution irrespective of its state. Thus  $J=1-0$ ,  $2-1$  are the CO lines where most observational calibrations of the so-called  $X_{\text{CO}} = \text{M}(\text{H}_2)/L_{\text{CO}}$  factor have been performed (see Bolatto et al. 2013, for a review). The two CI lines on the other hand are powerful alternatives for tracing the general  $\text{H}_2$  gas distribution (especially CI  $J=1-0$ ), often being brighter than CO  $J=1-0$ ,  $2-1$  in CO-rich gas while remaining luminous even in CO-poor gas (Papadopoulos et al. 2004).

Figure 2 plots the line-integrated intensities of the CO  $J=1-0$  and  $J=2-1$  transitions. It can immediately be seen that these intensities fall precipitously towards the CO-poor area. Indeed, their strengths relative to those typical in the CO-rich regions range from  $\sim 0.39$  at the “crossing” of the blue line (used to mark the CO-rich/CO-poor transition zone in the  $[\text{n}_{\text{H}} - \zeta_{\text{CR}}]$  parameter space), to only  $\sim 0.025-0.15$  deeper into the CO-poor regions in the upper left corner of the parameter space. Thus CO line observations conducted to yield the same S/N ratio for CO-poor molecular gas distributions would need  $\sim 7-1600$  longer integration time with respect to those of CO-rich regions. The CI  $J=1-0$ ,  $2-1$  lines on the other hand shown in Fig. 3, remain bright throughout most of the  $[\text{n}_{\text{H}} - \zeta_{\text{CR}}]$  parameter space, and actually much brighter than the two CO lines<sup>4</sup> This enables the two CI lines to

---

<sup>4</sup>This does not translate to  $I_{\text{CI}}/I_{\text{CO}} \times$  higher S/N ratios for CI versus CO observations as  $T_{\text{sys}}(\nu)$  will be higher at CI line frequencies. Nevertheless, significant gains in S/N are expected (e.g. Papadopoulos et al. 2004).

trace  $\text{H}_2$  gas both in CO-poor and CO-rich regions.

There is also an area of low CO *and* CI line intensities in the (high- $n_{\text{H}}$ )/(low- $\zeta_{\text{CR}}$ ) region of the  $[n_{\text{H}} - \zeta_{\text{CR}}]$  parameter space (lower right corner) in all plots of both Figs. 2 and 3. This is the area where non-SF, dense gas cores embedded deep into Galactic GMCs are located (e.g. Bok globules). These are very cold regions ( $T_{\text{gas}} \sim 10 \text{ K}$ ), and the reduction of CO  $J=1-0$ ,  $2-1$  line intensities with respect to the warmer gas in the (lower- $n_{\text{H}}$ )/(higher- $\zeta_{\text{CR}}$ ) areas almost purely reflects a temperature drop (since CO  $J=1-0$ ,  $2-1$  are thermalized and optically thick with  $E_{10,21}/(k_{\text{B}}T_{\text{gas}}) \lesssim 1$ ). The drop of the CI line intensity towards that area is due both to this temperature drop (that contributes non-linearly to the intensity reduction since for these lines  $E_{10,21}/(k_{\text{B}}T_{\text{gas}}) \gtrsim 1$ , especially for CI  $J=2-1$ ), and a  $[\text{C}/\text{CO}]$  abundance reduction. Nevertheless, given that such dense, cold gas cores contain only small mass fractions ( $\lesssim 1\%$ ) of Galactic GMCs, we do not anticipate that this (CO and CI)-dark region of  $[n_{\text{H}} - \zeta_{\text{CR}}]$  parameter space to be of any consequence when it comes to the inventory of  $\text{H}_2$  gas mass.

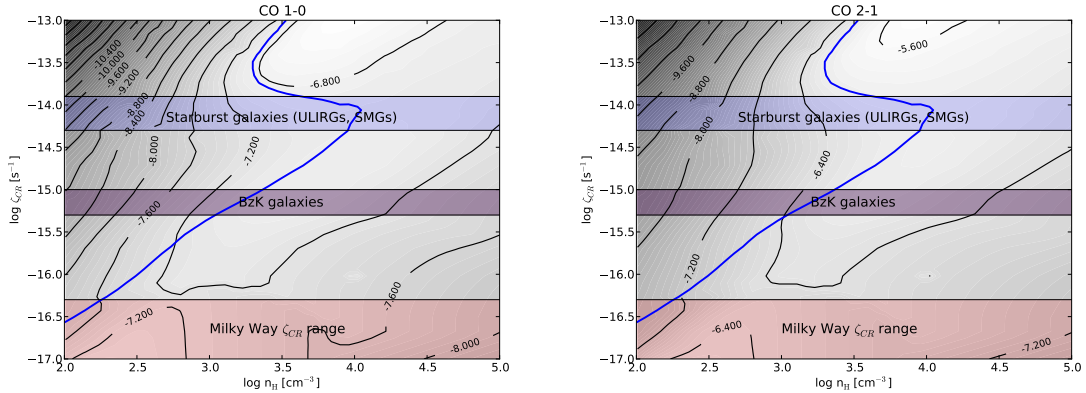


Fig. 2.— Logarithmic contour/grayscale plots showing the brightnesses of CO  $J=1-0$  (left) and CO  $J=2-1$  (right) in the  $[n_{\text{H}} - \zeta_{\text{CR}}]$  space. The brightness is calculated by integrating the local emissivity for a depth of  $A_{\text{V}} = 10 \text{ mag}$ , and is in units of  $\text{erg cm}^{-2} \text{ s}^{-1} \text{ sr}^{-1}$ . The blue line corresponds to  $\text{CO}/\text{H}_2 = 10^{-5}$  (see Fig. 1 for further details). The large reduction of the CO line strengths in the CO-poor regions is evident (see §2.1 for detailed discussion).

## 2.2. The effect of higher FUV fields

The choice of  $G = 0G_{\odot}$  in our calculations was driven by our intent to isolate the effect of CRs on the average  $[\text{CO}/\text{H}_2]$  abundance in molecular clouds. However ISM environments with higher SFR densities boost both the average  $\zeta_{\text{CR}}$  *and* the average FUV field  $G$ . Nev-

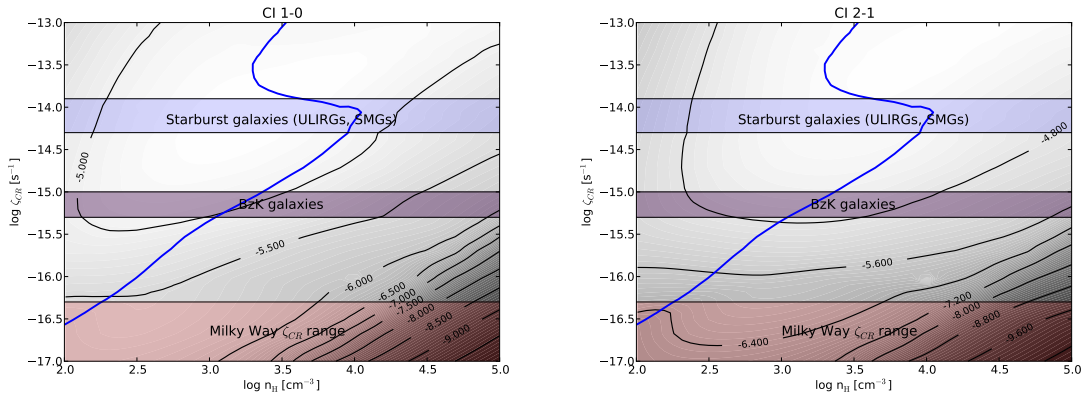


Fig. 3.— Logarithmic contour/grayscale plots showing C I  $J=1-0$  (left) and C I  $J=2-1$  (right) brightness in the  $[n_{\text{H}} - \zeta_{\text{CR}}]$  space. The brightness is calculated by integrating the local emissivity for a depth of  $A_{\text{V}} = 10$  mag, and is in units of  $\text{erg cm}^{-2} \text{s}^{-1} \text{sr}^{-1}$ . The blue line corresponds to  $\text{CO}/\text{H}_2 = 10^{-5}$  (see Fig. 1 for further details). The two C I lines remain luminous for much of the  $[n_{\text{H}} - \zeta_{\text{CR}}]$  space, even in CO poor regions. They become faint (as well as the CO  $J=1-0$ ,  $2-1$  lines) only for dense/cold gas with Galactic levels of  $\zeta_{\text{CR}}$  (see §2.1 for detailed discussion).

ertheless, unlike  $\zeta_{\text{CR}}$  the boost of the average FUV radiation field is much reduced by the dust absorption in the metal-rich ISM environments we study here. Indeed it is expected to be capped to  $G \sim 10^3 G_{\odot}$  (Papadopoulos et al. 2014), with higher values such as  $\sim 10^4 - 10^5$  associated with gas regions near O, B stars that contain only small mass fractions of molecular clouds. Furthermore, in environments of high gas turbulence (typical for ISM with high SFR densities, see also discussion in §5.1) such clouds are expected to have large  $\langle A_{\text{V}} \rangle$ , much larger than  $\langle A_{\text{V}} \rangle \sim 7 - 8$  found for Galactic GMCs (see Pelupessy et al. 2006). Thus we do not expect the  $[\text{CO}/\text{H}_2]$  to be affected by the average FUV fields for much of the molecular gas mass, a state of affairs which may, however, change for low-metallicity ISM. We must however note that increasing the FUV will result to a higher C II abundance (and C II line emission) in low densities.

We nevertheless still performed calculations for  $G = 10^3 G_{\odot}$  and  $G = 10^5 G_{\odot}$ , and found that the corresponding map shown in Fig. 1 to be in excellent agreement for  $A_{\text{V}} \geq 7$  mag. In addition, we compare the gas temperature of selected simulations with those studied in Meijerink et al. (2011) who included the effect of FUV radiation and also find excellent agreement.



### 2.3. Comparison with other theoretical models, and a $[\text{CO}/\text{H}_2]$ sensitivity on $T_{\text{gas}}$

As we noted in the Introduction, theoretical models by Bayet et al. (2011); Meijerink et al. (2011); Bialy & Sternberg (2014) have examined the effects of CRs in uniform density clouds, even if they did not focus on the CR-controlled  $[\text{CO}/\text{H}_2]$  abundance and its observational consequences in various extragalactic environments. Figure 4 shows a comparison between Bayet et al. (2011); Bialy & Sternberg (2014) and 3D-PDR results. Red and green lines compare 3D-PDR against Bialy & Sternberg (2014) respectively for isothermal runs at  $T_{\text{gas}} = 100$  K interacting with  $\zeta_{\text{CR}} = 10^{-16} \text{ s}^{-1}$ . It can be seen that the agreement is very good. We note that Bialy & Sternberg (2014) and the present work used different chemical network which can explain the discrepancy of the two curves for  $n_{\text{H}} < 2 \times 10^3 \text{ cm}^{-3}$ , while for  $n_{\text{H}} \geq 2 \times 10^3 \text{ cm}^{-3}$  the agreement is excellent. Switching on the thermal balance calculations (blue line) makes the  $\text{CO}/\text{H}_2$  ratio lower for  $n_{\text{H}} < 2 \times 10^3 \text{ cm}^{-3}$  while for  $n_{\text{H}} \sim 10^2 \text{ cm}^{-3}$  this ratio is  $< 10^{-5}$ , differing by an order of magnitude with respect to the isothermal runs. This demonstrates the importance of thermal balance calculations in estimating the effect of CRs on  $\text{CO}/\text{H}_2$  as the latter appears to have high sensitivity on gas temperature (see also §2.6). Lower temperatures form  $\text{O}_2$  via the reaction



which then reacts with C to form CO as shown in Reaction 12 (see §4.1), hence increasing the abundance of the latter.

The above reaction rate can be estimated using the following equation (e.g. Millar et al. 1997):

$$k = \alpha \left( \frac{T_{\text{gas}}}{300} \right)^{\beta} \left( e^{-\gamma/T_{\text{gas}}} \right), \quad (2)$$

with  $\alpha = 3.69 \times 10^{-11}$ ,  $\beta = -0.27$  and  $\gamma = 12.9$ . For  $T_{\text{gas}} = 14$  K (as obtained by the 3D-PDR runs),  $k = 3.36 \times 10^{-11}$  while for  $T_{\text{gas}} = 100$  K,  $k = 4.36 \times 10^{-11}$ . Hence at lower temperatures, such as those found by the thermal balance iterations in this work, the abundance of CO will be higher.

Finally, the yellow circular point corresponds to a simulation presented in Bayet et al. (2011) who included thermal balance calculations but used different chemical network and initial elemental abundances of species resulting in a discrepancy between their work and the present paper. By using the Bayet et al. (2011) initial elemental abundances, we obtain excellent agreement.

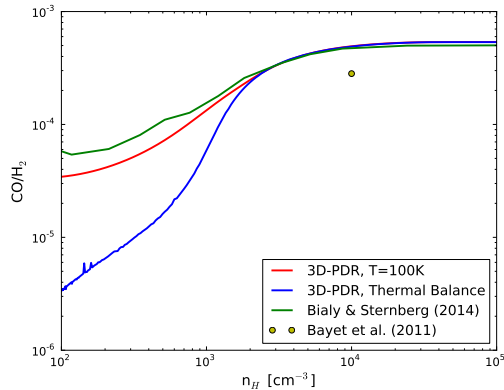


Fig. 4.— Comparison between 3D-PDR, Bayet et al. (2011); Bialy & Sternberg (2014). The cosmic-ray ionization rate is  $\zeta_{\text{CR}} = 10^{-16} \text{ s}^{-1}$ . The green line corresponds to the Bialy & Sternberg (2014) isothermal simulations and the red line mark our 3D-PDR isothermal calculations at  $T_{\text{gas}} = 100 \text{ K}$ . The blue line corresponds to the 3D-PDR calculations that solve also for gas thermal balance. The yellow circular point corresponds to a model by Bayet et al. (2011) for  $n_{\text{H}} = 10^4 \text{ cm}^{-3}$ . See §2 for the relevant discussion.

#### 2.4. A low-density CO/H<sub>2</sub> upwards turnover at high $U_{\text{CR}}$ values

The  $\text{CO}/\text{H}_2 = 10^{-5}$  contour marks a near-linear path across the  $[n_{\text{H}} - \zeta_{\text{CR}}]$  parameter space for up to  $\zeta_{\text{CR}} \sim 10^{-14} \text{ s}^{-1}$ . However, for higher  $\zeta_{\text{CR}}$  values there seems to be a “turnover” of this  $\text{CO}/\text{H}_2$  contour value towards lower densities, i.e. low-density gas starts becoming CO-rich again despite the now exceptionally high CR energy densities. We give a full description of the underlying chemistry of this behaviour in §4.1. We must note that although such CR-intense environments are too extreme to be considered representatives of average conditions in the ISM of SF galaxies, they could be possible locally near highly energetic CR-accelerating phenomena such as supernova explosions and young SNRs.

#### 2.5. A non-uniform cloud model embedded in a $1G_{\odot}$ FUV field

While our investigation using uniform density 3D-PDR models allows a clear overview of the density-dependence of the CR-induced destruction of CO, and what type of extragalactic environments would be most affected (see Fig.1), it is obviously too simple of an approach when it comes to individual molecular clouds where hierarchical density structures are known to exist. For the present work we choose to investigate the CR-controlled  $\text{CO}/\text{H}_2$  and  $\text{C I}/\text{CO}$  ratios for a cloud with a simple  $n_{\text{H}}(r) \propto r^{-1}$  profile. In the future we will use

the full capabilities of our 3D-PDR code where fractal density structures have been recently incorporated to examine the CR effects on the CO and CI abundances in much more realistic settings (i.e. such as those examined by Walch et al. 2012).

We consider a cloud with radius  $R = 20$  pc embedded in an environment with different cosmic-ray ionization rates. In particular, we perform a suite of runs in which we use a density profile following the Larson (1981) power law of  $n_{\text{H}}(r) \propto r^{-1}$  by adopting the density function

$$n_{\text{H}}(r) = \frac{4 \times 10^3}{0.04 + \left[\frac{r}{\text{pc}}\right]} \text{ cm}^{-3}. \quad (3)$$

The above density distribution has the following properties: the central core of the cloud reaches densities up to  $n_{\text{H}} = 10^5 \text{ cm}^{-3}$  while at  $R = 20$  pc it reaches densities down to  $n_{\text{H}} = 200 \text{ cm}^{-3}$ . The total mass of the cloud is  $M_{\text{TOT}} = 2.47 \times 10^5 M_{\odot}$  while its average density is  $\langle n_{\text{H}} \rangle \simeq 300 \text{ cm}^{-3}$ , typical of Galactic GMCs. We also include an external FUV radiation field of intensity  $G = 1G_{\odot}$ . Furthermore, the visual extinction at the centre of the core (measured from the edge of the sphere) is  $A_{V,\text{max}} \sim 50$  mags.

Figure 5 shows the results of the 3D-PDR calculations for different cosmic-ray ionization rates ( $\zeta_{\text{CR}} = 10^{-17} - 10^{-14} \text{ s}^{-1}$ ). We can now see the effects of enhanced CRs within an inhomogeneous  $\text{H}_2$  cloud. The red line marks a  $\text{CII}/\text{CI}=5$  ratio, with the spherical shell outside that line (i.e. outer part) consisting almost entirely of CII. The green line corresponds to  $\text{CI}/\text{CO}=5$  hence the shell between the red and green lines is CI-dominated while the rest of the cloud (i.e. inner to the green line) is CO-dominated. The blue line defines the  $\text{CO}/\text{H}_2 = 10^{-5}$  ratio and hence the maximum volume where CO can easily trace  $\text{H}_2$ . Finally, we also plot the  $\text{HI}/2\text{H}_2=1$  ratio with a black line (visible only in Panel D). The volume inner to that line is  $\text{H}_2$ -dominated, with the outer part where CRs have mostly destroyed  $\text{H}_2$  to form HI.

In Table 1 we list the  $\text{H}_2$  gas mass fractions traceable by CO, CI and CII in each case. We find that CII *cannot trace more than 1% of the cloud in any of the cases*. As  $\zeta_{\text{CR}}$  increases, the  $\text{H}_2$  gas becomes CI-rich as CO gets destroyed by the reaction with  $\text{He}^+$ . At  $\zeta_{\text{CR}} = 10^{-16} \text{ s}^{-1}$  only  $\sim 33\%$  remains CO-rich while for  $\zeta_{\text{CR}} \geq 10^{-15} \text{ s}^{-1}$  most of the cloud is CO-poor (but CI-rich). Evidently, cosmic rays play a major role in controlling the CO-visibility of  $\text{H}_2$  gas while leaving the CI lines as the only alternative molecular gas mass tracers.

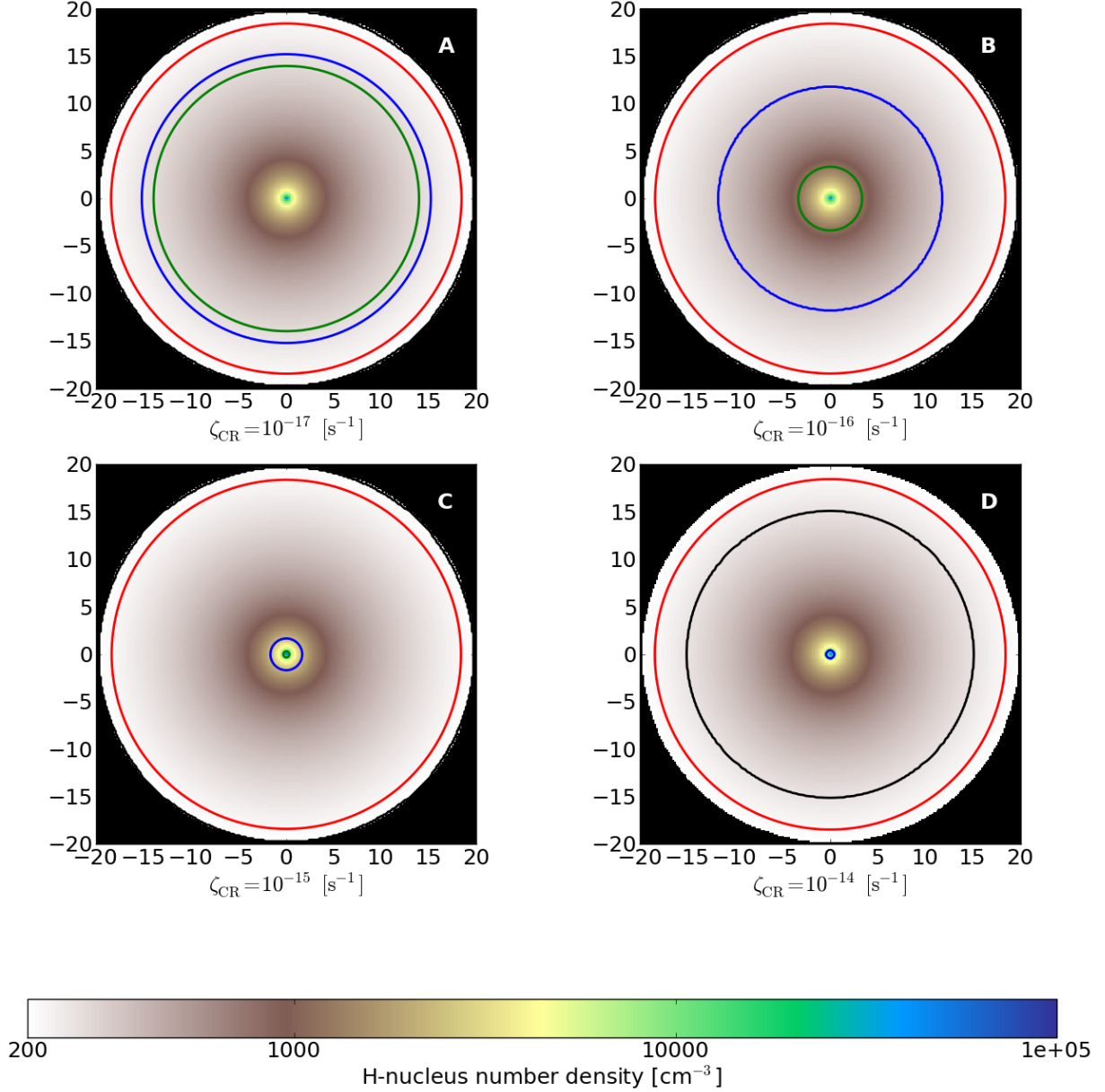


Fig. 5.— The spherically symmetric one-dimensional simulation for the cloud with density profile as described in Eqn.3. Each different panel corresponds to different  $\zeta_{\text{CR}}$ . From A to D,  $\zeta_{\text{CR}} = 10^{-17}, 10^{-16}, 10^{-15}, 10^{-14} \text{ s}^{-1}$ . The colour bar corresponds to the  $n_{\text{H}}$  number density. The red line corresponds to  $\text{CII}/\text{CI}=5$ . The blue line corresponds to  $\text{CO}/\text{H}_2 = 10^{-5}$ , whereas the green one to  $\text{CI}/\text{CO}=5$ . The black line (which is only visible in the D panel because in all other cases it lies in the edge of the cloud), corresponds to  $\text{HI}/2\text{H}_2 = 1$ .  $\text{H}_2$  is traceable by CO and CI in the region below the blue line; by CI only in the region between the red and the blue line; and by CII only in the region outside the red line. For the particular case of panel D,  $\text{H}_2$  is traceable by CI only in the inner area of the cloud.

### 2.6. The importance of thermal balance

We will now briefly explore the effects of thermal balance on the results of this work. To do this, we switch off the thermal balance iteration scheme in 3D-PDR and instead we run two isothermal grids of runs. Figure 6 plots the CO/H<sub>2</sub> ratio in the  $n_{\text{H}}$  and  $\zeta_{\text{CR}}$  parameter space for  $T_{\text{gas}} = 20$  K (left panel) and  $T_{\text{gas}} = 100$  K (right panel). The thick solid line corresponds to CO/H<sub>2</sub> = 10<sup>-5</sup>. In both cases, the CO/H<sub>2</sub> ratio follows a linear behaviour with  $\log n_{\text{H}}$  and  $\log \zeta_{\text{CR}}$  thus demonstrating that the dependence of the chemical reactions on the gas temperature in such cosmic-ray dominated environments is a highly non-linear and at the same time a very important one. Indeed Bialy & Sternberg (2014), which used an analytical approach (and simpler chemical pathways) along with an isothermal assumption (at  $T_{\text{gas}} = 100$  K), do not recover this behavior, nor do they find the large reduction of CO/H<sub>2</sub> at high CR energy densities.

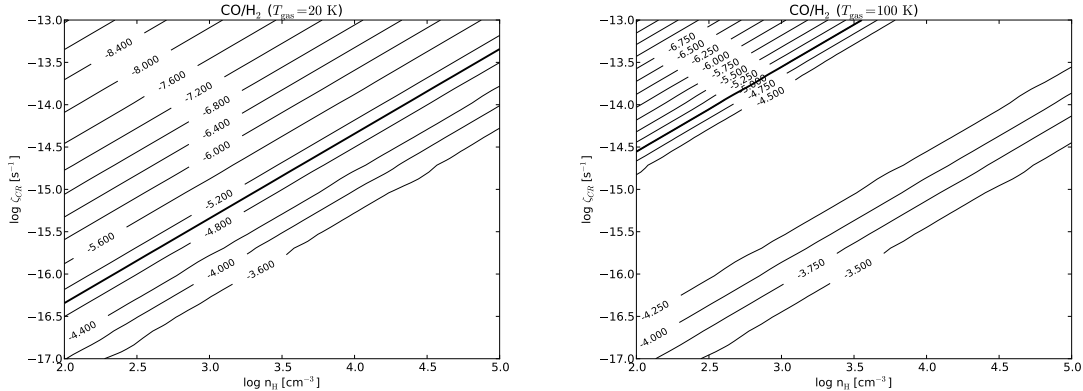


Fig. 6.— The CO/H<sub>2</sub> ratio for the isothermal runs discussed in §2.6. The left panel shows the resultant contour plot for  $T_{\text{gas}} = 20$  K and the right panel for  $T_{\text{gas}} = 100$  K (c.f. Bialy & Sternberg 2014). The thick solid line corresponds to CO/H<sub>2</sub> = 10<sup>-5</sup>. A strong dependency on the gas temperature is apparent, with the highest temperatures corresponding to much smaller suppressions of the CO/H<sub>2</sub> abundance ratio. This demonstrates the importance of solving for the detailed thermal balance.

### 3. A secondary effect: clumpy low- $J$ CO emission in gas-rich SF disks?

A secondary effect that may occur in H<sub>2</sub>-rich galactic disks permeated by high  $U_{\text{CR}}$  backgrounds (boosted by the intense star formation typically hosted by such disks) which destroy CO more effectively at lower gas densities *is to make such disks appear clumpy in*

*low- $J$  CO line emission*<sup>5</sup>. This can occur simply because the CR-induced destruction of CO, being more effective at lower densities, will leave only smaller and denser parts of molecular clouds to be CO-rich. The appearance of such clouds or cloud ensembles via their low- $J$  CO line emission will then be much clumpier, depending on the average  $U_{\text{CR}}$  background and the underlying mass-density  $dM_{\text{gas}}(n)/dn$  function of the molecular clouds. Finally, if lower density molecular clouds lie preferably at larger galactocentric distances, such CR-inundated molecular gas disks could appear more compact in low- $J$  CO emission than they actually are. Such large scale CR-induced effects on the (CO-line)-visibility of the  $\text{H}_2$  gas distribution in galaxies can only be accentuated once metallicity gradients (with lower-metallicity gas found preferably at larger galactocentric distances) are also taken into account (see also §5.1).

There are now several deep CO  $J = 1 - 0, 2 - 1$  images available for gas-rich SF systems in the distant Universe (e.g. Daddi et al. 2010; Ivison et al. 2010; Riechers et al. 2011; Hodge et al. 2012), with clumpy gas disks often claimed (e.g. Hodge et al. 2012). In such cases it would be interesting to also conduct deep CI  $J=1-0, 2-1$  line imaging since CI is a by-product of the CR-induced CO destruction which remains abundant also in CO-rich molecular gas. Thus it can then trace any CO-dark  $\text{H}_2$  gas along with its CO-rich phase (see Fig.1), and may thus reveal smoother  $\text{H}_2$  gas distributions in CR-permeated SF disks than the CO  $J=1-0, 2-1$  lines.

On the theoretical front, hydrodynamical simulations of gas-rich disks with: a) high enough resolution to track the molecular cloud turbulence (which sets their  $dM_{\text{gas}}(n)/dn$ ) and b) detailed  $\text{H}_2, \text{CO}$  formation/destruction chemical networks, can elucidate whether CRs can induce such a bias on the structural characteristics of  $\text{H}_2$ -rich disks derived from CO  $J=1-0, 2-1$  lines (see also §5.2).

#### 4. A chemical and analytical determination of the CO-dark $\text{H}_2$ domain

A main result of this study is the discovery of a large area in the  $[n_{\text{H}} - \zeta_{\text{CR}}]$  parameter space where gas is mostly molecular but CO-poor. In this Section we identify the responsible chemical pathways for this behaviour, then attempt to find an analytical equation that could be used in purely (hydro-)dynamical codes for determining the average CO/ $\text{H}_2$  ratio as a function of gas density and  $\zeta_{\text{CR}}$  in turbulent molecular gas clouds.

---

<sup>5</sup>Molecular gas disks in CO  $J = 3-2$  and higher- $J$  CO line emission *are* expected to appear much clumpier than in CO  $J = 1 - 0, 2 - 1$  because high- $J$  CO lines sample only the more compact dense and warm gas regions near SF sites while CO  $J=1-0, 2-1$  are expected to trace the entire molecular gas distribution (as long as it is CO-rich).

#### 4.1. The chemistry of H<sub>2</sub> and CO

While the *main* chemical formation and destruction routes of both H<sub>2</sub> and CO in the gas phase are very well known, in order to understand the region in the  $[n_{\text{H}} - \zeta_{\text{CR}}]$  plane of Fig.1 where CO is destroyed but H<sub>2</sub> is not, one needs to take into consideration several more chemical reactions as a function of these two parameters. We perform a chemical analysis of three representative such models outlining that region (their properties in tabulated in Table 2 and the rates used for the reactions presented below are shown in Table 3). We note, however, that the chemical pathway and particularly the efficiency of the reaction rates follows a non-linear behavior, therefore the analysis below is very model-dependent and hence should be taken as qualitative.

In M1 and M2, H<sub>2</sub> is mainly formed by the ion-neutral reaction:



which contributes  $\sim(70-90)$  % to the formation of H<sub>2</sub>. For the formation of H<sub>2</sub> the behaviour is similar for the model M3, with the difference that the ion-neutral reactions forming H<sub>2</sub> are:



H<sub>2</sub> is then destroyed *in almost equal efficiencies* by recombination and cosmic rays ionization in all models:



Hence cosmic rays, although an efficient mean of destruction, are not necessarily the dominant route. CO on the other hand is formed mainly via neutral-neutral reactions in M1, with the two most efficient ( $\sim 30\%$  each) routes being:



with some contribution ( $\sim 15\%$ ) from:



Table 1: This table shows the amount (%) of H<sub>2</sub> gas which is traceable by CO, CI and CII for the four simulations presented in §2.5. The first column corresponds to the panels of Fig.5. The second column corresponds to the intensity of CRs and the third column to the H<sub>2</sub> gas mass. The rest of columns correspond to the amount of H<sub>2</sub> that is CO, CI, and CII bright i.e. traceable by these elements. It can be seen that once we increase the  $\zeta_{\text{CR}}$  value CI becomes the most important tracer for H<sub>2</sub>.

Panel	$\zeta_{\text{CR}} [\times 10^{-17} \text{ s}^{-1}]$	H <sub>2</sub> [ $\times 10^5 M_{\odot}$ ]	CO & CI (%)	CI (%)	CII (%)
A	1	2.47	~55	~44	<1
B	10	2.47	~33	~76	<1
C	10 <sup>2</sup>	2.47	<1	~99	<1
D	10 <sup>3</sup>	1.38	<0.1	>99.9	N/A

Table 2: Properties of three representative models marking the outlines of CO-poor/H<sub>2</sub>-rich region.

Model ID	$\log n_{\text{H}} (\text{cm}^{-3})$	$\log \zeta_{\text{CR}} (\text{s}^{-1})$
M1	2.5	-16
M2	2.5	-15
M3	3.5	-15



Table 3: Reaction rates for the chemical analysis discussed in §4.1.

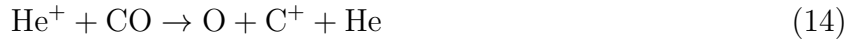
Reaction	$\alpha$	$\beta$	$\gamma$
4	$6.40 \times 10^{-10}$	0.0	0.0
5	$7.98 \times 10^{-10}$	-0.16	1.4
6	$2.00 \times 10^{-9}$	0.0	0.0
7	$1.36 \times 10^{-9}$	0.0	0.0
8	$1.20 \times 10^{-17}$	0.0	0.0
9	$2.08 \times 10^{-9}$	0.0	0.0
10	$6.02 \times 10^{-11}$	0.1	-4.5
11	$1.00 \times 10^{-10}$	0.0	0.0
12	$5.56 \times 10^{-11}$	0.41	-26.9
13	$7.50 \times 10^{-10}$	0.0	0.0
14	$1.60 \times 10^{-9}$	0.0	0.0

In M2, the Reaction 12 is not important but the rest of CO is formed via the ion-neutral reaction:



Interestingly, in M3 CO forms only via the neutral-neutral reactions listed above (i.e. Reactions 10–12).

However, *in all models CO is always very efficiently destroyed indirectly by cosmic rays, via  $\text{He}^+$*  (which forms via cosmic ray ionization) with the reaction:



It therefore seems that a main reason for a CO-dark  $\text{H}_2$  phase is that a higher cosmic ray ionization rate drives a higher rate of destruction of CO, but has a much less dramatic effect on  $\text{H}_2$ . It is worth noting here that  $\text{He}^+$  can be destroyed by reacting with  $\text{H}_2$ ; this reaction has a small barrier leading to its rate coefficient becoming a factor of two higher at 100 K (i.e. the gas temperature that Bialy & Sternberg 2014, considered) than at 40 K (i.e. the gas temperature of the M3 model), possibly reducing  $\text{He}^+$  enough to allow CO to survive at higher abundances. A thorough investigation of the chemistry, as a function of temperature, that can lead to a CO-poor/ $\text{H}_2$ -rich environment is beyond the scope of this paper but it is clear that chemistry resulting from a high cosmic ray ionization rate when thermal balance is taken into account is not easily determined a priori.

Fig.1 also shows a high  $\zeta_{\text{CR}}$  regime with a small parameter space where the general trend of (higher- $\zeta_{\text{CR}}$ ) $\rightarrow$ (higher-n gas becoming CO-poor) is reversed. In the left panel of Fig.7 we

now show how CO/H<sub>2</sub> varies with increasing ζ<sub>CR</sub> for three different number densities, while the right panel shows the corresponding gas temperatures. The left panel of Fig.7, for a density range n<sub>H</sub> = 10<sup>3</sup> – 10<sup>4</sup> cm<sup>-3</sup> and ζ<sub>CR</sub> ≥ 3 × 10<sup>-15</sup> s<sup>-1</sup>, shows the reversal of the aforementioned trend, with high-density gas becoming CO-rich again despite the now very high ζ<sub>CR</sub> values. This reversal is much less prominent for low-density gas. We ran a chemical analysis for these models and we found that He<sup>+</sup> is efficiently (by > 50%) destroyed by:



where M stands for metals for which we used a total elemental fractional abundance of 4 × 10<sup>-5</sup> (Asplund et al. 2009). Note that Reaction 15 is not very efficient in models where CO decreases with cosmic ray ionization rate.

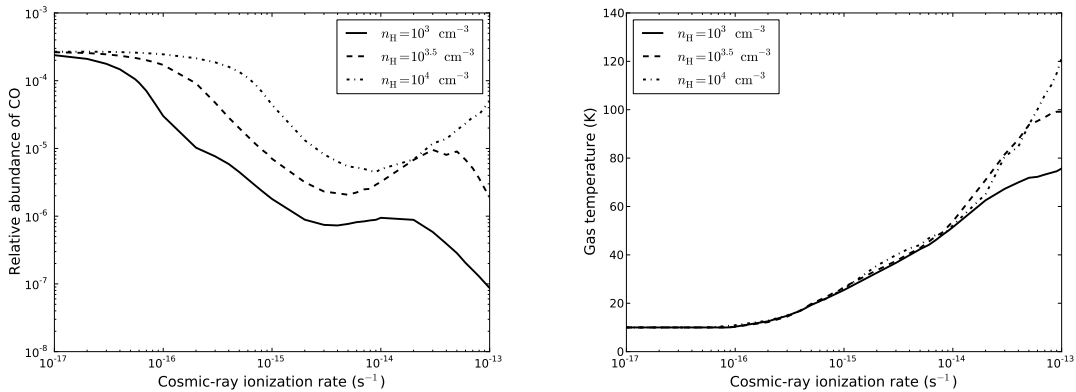


Fig. 7.— The left panel shows the abundance of CO (relative to hydrogen) versus the cosmic-ray ionization rate (ζ<sub>CR</sub>) for three different densities ( $n_{\text{H}} = 10^3 \text{ cm}^{-3}$  solid line,  $n_{\text{H}} = 10^{3.5} \text{ cm}^{-3}$  dashed line, and  $n_{\text{H}} = 10^4 \text{ cm}^{-3}$  dot-dashed line). For  $\zeta_{\text{CR}} \gtrsim 10^{-14} \text{ s}^{-1}$  we observe an increase of CO abundance due to the destruction of He<sup>+</sup> (see §4.1). The right panel shows the corresponding gas temperature which increases with increasing ζ<sub>CR</sub>.

Nevertheless such extreme CR-permeated gas regions where this effect can take place are unlikely to be representative of average ISM conditions even in the most extreme merger/starbursts known, yet they could be found near or within young SNRs. In such a case the effect described here may indicate the survival of the CO molecule in dense molecular gas within some truly extreme CR-dominated regions.

## 4.2. An analytical approximation of the the CO-dark H<sub>2</sub> domain

The left panel of Fig.8 is a contour plot showing 3D-PDR results of the  $\log(\text{CO}/\text{H}_2)$  as a function of  $n_{\text{H}}$  and  $\zeta_{\text{CR}}$ . The following function is best fit to our data:

$$\begin{aligned} \log(\text{CO}/\text{H}_2) = & -110.7 + 28.69 \log n_{\text{H}} \\ & -12.82 \log \zeta_{\text{CR}} - 1.512(\log n_{\text{H}})^2 \\ & +2.642 \log n_{\text{H}} \log \zeta_{\text{CR}} - 0.5377(\log \zeta_{\text{CR}})^2 \\ & -0.08047(\log n_{\text{H}})^2 \log \zeta_{\text{CR}} \\ & +0.06209 \log n_{\text{H}}(\log \zeta_{\text{CR}})^2 - 0.008312(\log \zeta_{\text{CR}})^3 \end{aligned} \quad (16)$$

and is plotted in the right panel of Fig.8. This equation is applicable for negligible FUV radiation within a cloud, typically for  $A_{\text{V}} \geq 7$  mag (the case for most H<sub>2</sub> gas mass in starbursts). In cases where FUV radiation is significant this parametric equation still provides a *maximum* CO/H<sub>2</sub> abundance ratio possible for a given average SFR density (since FUV can only destroy CO further while leaving the mostly self-shielding H<sub>2</sub> intact).

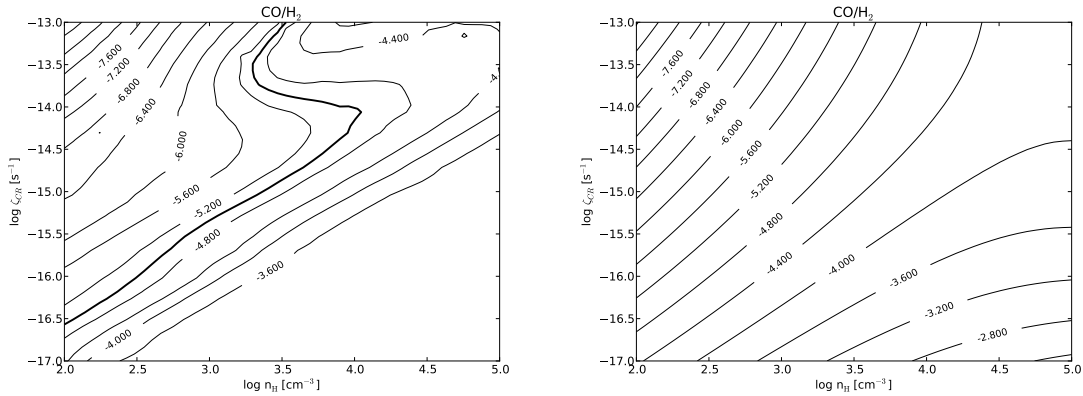


Fig. 8.— The left panel of the figure shows a contour plot of the 3D-PDR results for the CO/H<sub>2</sub> ratio. The thick solid line corresponds to  $\text{CO}/\text{H}_2 = 10^{-5}$ . The right panel shows the corresponding best fit function described in Eqn.16.

This relation cannot track the behaviour of CO/H<sub>2</sub> as extracted from the detailed 3D-PDR models in some domains (e.g. at  $n_{\text{H}} \sim 1000 \text{ cm}^{-3}$  and very high cosmic ray ionization). However for the  $[n_{\text{H}} - \zeta_{\text{CR}}]$  parameter space where most of the molecular gas mass of SF galaxies is expected to be this relation gives reasonably good results<sup>6</sup>. It can then be used in

---

<sup>6</sup>The coefficients have a 95% confidence bounds, and a Mean Squared Error (MSE) analysis on this function yields an MSE of 0.04; and as Mean Absolute Percentage error (MAPE) of 3.5%.

galaxy-sized or cosmology-sized hydrodynamic simulations of atomic and molecular gas and stars where the underlying molecular cloud physics is treated in a sub-grid fashion (Pelupessy & Papadopoulos 2009; Narayanan et al. 2011; Lagos et al. 2012; Christensen et al. 2012). Such simulations are frequently used to predict the CO-deduced versus the true  $\text{H}_2$  gas distributions in galaxies (e.g. Pelupessy & Papadopoulos 2009) or make predictions of CO line luminosities of galaxies in a cosmological setting (e.g. Lagos et al. 2012). Yet none currently takes into account the expected strong effects of CRs, driven by the often high and strongly evolving SFR densities found in the Early Universe.

In the case of cosmological simulations used to predict CO SLEDs for galaxies in a  $\Lambda$ CDM universe (e.g. Lagos et al. 2012) knowing the temperature of CR-heated gas in the CO-rich and CO-poor phases is also important. In Fig.9 we show the temperatures attained by the molecular gas within the  $[n_{\text{H}} - \zeta_{\text{CR}}]$  parameter space explored. Finally, from our work it is now clear that  $\text{Cl } J=1-0, 2-1$  line emission is important for recovering the CO-poor  $\text{H}_2$  gas distribution along with the CO-rich one in galaxies. Cosmological simulations of  $\text{Cl}$  line luminosities in galaxies have been recently published (Tomassetti et al. 2014), but without taking into account the important effects of CRs in regulating the  $\text{CO}/\text{H}_2$  and  $\text{Cl}/\text{H}_2$  abundance ratios.

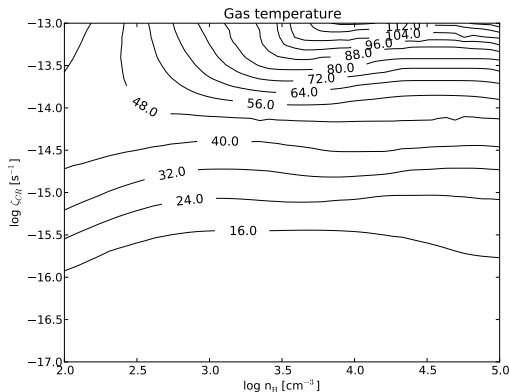


Fig. 9.— Contours showing the corresponding gas temperatures for the parameter space shown in Fig.1. From this Figure it is also obvious that most of the temperatures attained by the gas are well below the temperature assumed by Bialy & Sternberg (2014) their isothermal treatment.

## 5. Discussion

Quite unlike the FUV radiation fields incident on molecular clouds, CRs can destroy CO equally efficiently throughout their volume rather than mostly at outer cloud layers. CRs can thus be the main regulator of the CO-“visibility” of molecular gas in SF galaxies with the FUV-induced CO destruction a secondary one. Only for low-metallicity molecular gas in high-intensity radiation the FUV-induced CO destruction can surpass the CR-induced one. Nevertheless, given that high average FUV fields are found in places of elevated SFR densities, and thus also of boosted  $U_{\text{CR}}$ , the two effects will always operate in parallel, even as the average FUV radiation fields will not follow the rise of  $\zeta_{\text{CR}}$  to high values in a proportional manner in metal-rich SF environments (see Papadopoulos et al. 2014, for details).

In future work we will explore the combined effects of high  $G_{\circ}$  and  $\zeta_{\text{CR}}$  on molecular gas with a range of metallicities. Given the non-linear effects behind the FUV-induced and CR-induced CO destruction, these may be much more dramatic than either effect alone. FUV-intense environments with low average metallicities will be typical in the early Universe, either over entire galaxies (e.g. Ly-break galaxies, dwarfs) or in the outer, metal-poor, parts of SF disks in the process of building up their present-epoch  $Z(R)$  gradients.

### 5.1. Two caveats: CR penetration, and the effects of turbulence

Our analysis has been based on the assumption that  $U_{\text{CR}} \propto \rho_{\text{SFR}}$ , and that CRs penetrate into most of the volume of molecular clouds. There are good observational and theoretical arguments supporting both these assumptions, reviewed in Papadopoulos (2010). Briefly, the first assumption underlies the so-called far-IR/radio correlation established for galaxies whose radio and far-IR emission are powered by star formation, while the second one is supported by  $\gamma$ -ray observations of  $\text{H}_2$ -rich starbursting galactic centers, and by the thermal, ionization, and chemical states observed for FUV-shielded dense molecular gas cores in the Galaxy (Bergin & Tafalla 2007). Finally, if CRs were unable to penetrate deep inside the FUV-shielded regions of molecular clouds there would be no molecules present other than  $\text{H}_2$  since CRs, by driving the  $\text{H}_3^+$  formation in such regions, initiate the chemical network beyond the basic  $\text{H}_2$  molecule (itself formed on dust grains).

The effects of strong turbulence on a CR-controlled CO/ $\text{H}_2$  ratio, and its consequences for the CO-“visibility” of  $\text{H}_2$  gas in SF galaxies, are difficult to assess within the static framework of our work. The necessity of a dynamical approach can be shown simply by noting that the turbulent diffusion timescales  $t_{\text{diff}}$  are typically shorter than chemical-equilibrium timescales  $t_{\text{ch}}$ , the latter approximated by the timescale needed for an  $\text{HI}/\text{H}_2$

equilibrium to be reached (e.g. Hollenbach & Tielens 1999). Indeed for an initially atomic Cold Neutral Medium (CNM) phase (and a canonical  $\text{H}_2$  formation rate on grains of  $R_f = 3 \times 10^{-18}(\text{T/K})^{-1/2}\text{cm}^3\text{s}^{-1}$ ) it is  $t_{\text{ch}} \sim 10^7$  yrs, while  $t_{\text{diff}} \propto 1/K_{\text{diff}}$  (with  $K_{\text{diff}} = \langle V_{\text{turb}}L \rangle \sim (10^{24} - 10^{25})\text{cm}^2\text{s}^{-1}$ , Xie et al. 1995) ranges from  $t_{\text{diff}} \sim 3 \times 10^6$  yrs for quiescent GMCs (turbulent linewidths of  $V_{\text{turb}} \sim (1 - 5)\text{km s}^{-1}$ ) to  $\sim 3 \times (10^4 - 10^5)$  yrs for clouds typical of ULIRG environments (Papadopoulos et al. 2004, and references therein) The supersonic turbulence that dominates the velocity fields of molecular clouds is expected to influence our results in two distinct ways namely: a) by strongly “mixing” outer and inner cloud layers (and thus also the respective abundances of the various species formed in those cloud regions), and b) by controlling the molecular cloud mass fraction over the gas density range i.e. the  $dM_{\text{gas}}/dn$  function (Vazquez-Semadeni 1994; Padoan & Nordlund 2002, and references therein). Early work on the first issue by Xie et al. (1995) indicates that it is the abundances established on the outer cloud layers (i.e. the CO-poor/CI-rich ones in CR-immersed clouds with realistic density profiles) that will act to “dilute” the inner, denser, CO-rich/CI-poor regions. Furthermore, the typically stronger turbulence of the outer lower-density molecular cloud regions with respect to the inner more quiescent ones can only enhance such turbulent diffusion transfer of outer layer abundances inwards. These effects would then further reduce the CO-visibility of turbulent molecular clouds immersed in high CR energy density backgrounds.

Regarding the second issue, we note that galaxies with high average  $\rho_{\text{SFR}}$  values like ULIRGs are typically also those with much higher levels of turbulence (and hence dense gas mass fractions which in turn “fuel” their high  $\rho_{\text{SFR}}$ ). Indeed the face-on velocity dispersion of the molecular gas disks in ULIRGs is  $\sigma(V_z) \sim (30-140)\text{km s}^{-1}$  (Downes & Solomon 1998), much higher than in isolated spiral disks ( $\sim 10\text{km s}^{-1}$ ). As a result the underlying  $dM_{\text{gas}}/dn$  would “shift” most of the mass of a molecular cloud towards high densities ( $\geq 10^4\text{cm}^{-3}$ ), and thus towards the CO-rich part of the  $[n_{\text{H}} - \zeta_{\text{CR}}]$  parameter space shown in Fig.1, perhaps despite the also high average  $\zeta_{\text{CR}}$  expected in such environments. Only hydrodynamical simulations of molecular clouds with such high levels of turbulence *and* the appropriate chemical networks for CO and  $\text{H}_2$  formation and destruction can decide this issue. On the other hand it is worth pointing out that the cm-emission synchrotron disks of galaxies (rough indicators of the extend of CR propagation) are typically larger than the CO-visible molecular gas distributions. Thus starburst-originating CRs may affect the CO/ $\text{H}_2$  ratio beyond the starburst region itself, where lower-density, non-SF, molecular clouds may lie.

## 5.2. Some observational tests

A mainly CR-controlled CO/H<sub>2</sub> ratio in the molecular clouds of SF galaxies has some interesting observational consequences, which can be probed using the JVLA and ALMA, the two interferometer arrays operating in cm and mm/submm wavelengths with high sensitivities. The JVLA can image the cm synchrotron radiation emitted by CR electrons (and thus serve as a probe of CR propagation through galactic disks and individual molecular clouds), while ALMA can image the spectral lines of various species emanating from CR-permeated molecular gas, to yield tests of a CR-controlled chemistry. More specifically:

1. Deep imaging of the cm continuum of gas-rich SF disks along with CO  $J=1-0$ ,  $2-1$  and C<sub>I</sub>  $J=1-0$ ,  $2-1$  line imaging can reveal the distribution of CR-permeated molecular gas, and probe the structural characteristics of the molecular gas distribution as recovered via C<sub>I</sub> lines versus those using the two low- $J$  CO lines.
2. Imaging of individual molecular clouds in nearby SF galaxies in cm synchrotron continuum as well as in CO  $J=1-0$ ,  $2-1$  and C<sub>I</sub>  $J=1-0$ ,  $2-1$  lines in order to examine the effects of CRs in individual GMCs.
3. Any molecular line observations constraining the average  $x(e)$  (ionization fraction) within molecular clouds, versus CR distribution (traced by cm continuum imaging), can reveal whether CRs penetrate throughout GMC volumes determining their chemistry (e.g.  $x(e)$  correlating with cm emission brightness).

Generally in high CR energy density environments we expect H<sub>2</sub> clouds to be marked by the usual CO-bright emission emanating from the regions that are dense enough to retain their CO-richness, *yet having C<sub>I</sub> line emission extending much further out than those CO-bright regions*, tracing a CO-poor phase where CO has been destroyed by CRs. Given the elevated temperatures of the latter phase (see Figs.7 & 9) we expect both the C<sub>I</sub>  $J=1-0$  ( $E_{10}/k_B \sim 24$  K) and C<sub>I</sub>  $J=2-1$  ( $E_{21}/k_B \sim 62$  K) to be substantially excited. In principle this allows C<sub>I</sub> line imaging observations of SF disks to access a larger co-moving volume of the Universe and serve as alternative H<sub>2</sub> gas distribution tracers.

## 6. Conclusions

In this paper we examined the impact of CRs on the average CO/H<sub>2</sub> ratio in H<sub>2</sub> clouds. We find that even ordinary boosts of CR energy densities, expected in numerous SF galaxies in the Universe, can destroy CO (but not H<sub>2</sub>), so effectively as to render potentially large H<sub>2</sub>

gas reservoirs CO-poor and difficult to trace using conventional CO  $J=1-0$ ,  $2-1$ , line imaging. This is a density-dependent effect, with denser regions able to retain higher CO/H<sub>2</sub> ratios than low-density ones, for a given CR energy density (and thus CR ionization rate). This may give rise to a second order effect with H<sub>2</sub> gas disks that host vigorous SF, appearing clumpier in CO  $J=1-0$ ,  $2-1$  emission than they really are, their denser (and clumpier) H<sub>2</sub> gas regions having retained large enough CO/H<sub>2</sub> ratios as to remain CO-visible, unlike the CO-poor lower-density ones. Furthermore, even for CR energy density backgrounds expected in the Milky Way, low-density gas ( $n_{\text{H}} \sim 1 - 3 \times 10^2 \text{ cm}^{-3}$ ) can also be very CO-poor. The CR-induced destruction of CO leaves behind a CI-rich molecular gas phase, with only small amounts of CII. The CI  $J=1-0$ ,  $2-1$  lines are then the only remaining effective H<sub>2</sub> mass distribution tracers, encompassing both for the CO-rich and the CO-poor phase.

Strong turbulence, often found for the molecular gas of vigorously SF galaxies, can in principle help maintain much of it CO-rich (and thus CO-line-visible), by placing most of it at high average densities. Hydrodynamical simulations of highly turbulent, CR-irradiated molecular gas, which incorporate the appropriate CO, H<sub>2</sub> formation/destruction chemical networks, are necessary to explore this issue. On the observational front deep CI, low- $J$  CO line, and cm continuum imaging observations of SF galaxies and individual molecular clouds embedded in environments of high  $U_{\text{CR}}$ , are key in exploring a CR-regulated CO/H<sub>2</sub> ratio in H<sub>2</sub> clouds. We expect the CI line emission to extend well beyond that of low- $J$  CO line emission if that is indeed so.

We thank the anonymous referee for suggestions that improved a previous version of the manuscript and enlarged its scope. The work of TGB was funded by STFC grant ST/J001511/1. The work of PPP was funded by an Ernest Rutherford Fellowship. The authors thank Antonios Makrymallis for his contribution on calculating Eqn.16. TGB and PPP thank Nikos Karafolas and Despoina Gika for their hospitality at Seli (and the pita in particular), Veroia, where principal ideas of the present paper have been discussed. This research has made use of NASA’s Astrophysics Data System.

Parts of the calculations of the present paper used the DiRAC Data Analytic system at the University of Cambridge, operated by the University of Cambridge High Performance Computing Service on behalf of the STFC DiRAC HPC Facility ([www.dirac.ac.uk](http://www.dirac.ac.uk)). This equipment was funded by BIS National E-infrastructure capital grant (ST/K001590/1), STFC capital grants ST/H008861/1 and ST/H00887X/1, and STFC DiRAC Operations grant ST/K00333X/1. DiRAC is part of the National E-Infrastructure.



## A. The numerical model

We use 3D-PDR (Bisbas et al. 2012), a three-dimensional time-dependent astrochemistry code implemented at University College London and designed for treating PDRs of arbitrary density distribution. The code has been used in various applications examining galactic and extragalactic objects (i.e. Offner et al. 2013, 2014; Bisbas et al. 2014; Gaches et al. 2014). For the purposes of this work, we perform high resolution one-dimensional uniform-density clouds as discussed in Bisbas et al. (2012). We use a subset of the UMIST 2012 network (McElroy et al. 2013) consisting of 58 species and more than 600 reactions. The abundances of species relative to hydrogen we used are  $[\text{He}] = 8.5 \times 10^{-2}$ ,  $[\text{C}] = 2.69 \times 10^{-4}$ ,  $[\text{O}] = 4.90 \times 10^{-4}$ ,  $[\text{Mg}] = 3.98 \times 10^{-5}$ , and  $[\text{S}] = 1.32 \times 10^{-5}$  which correspond to undepleted solar abundances (Asplund et al. 2009). Full technical details can be found in Bisbas et al. (2012) and in Bisbas et al. (2014) for further updates.

In the simulations presented here, we use an expression for molecular line optical depths suitable for macroturbulent molecular clouds. Thus in the expression of  $\tau_{ij}$  for the line transition  $ij$  of

$$\tau_{ij} = \frac{A_{ij}c^3}{8\pi\nu_{ij}^3} \left( \frac{dV}{dr} \right)_{\text{VIR}}^{-1} \left[ \frac{n_j g_i - n_i g_j}{g_j} \right], \quad (\text{A1})$$

(where  $A_{ij}$  is the Einstein coefficient,  $\nu_{ij}$  is the line frequency,  $n_i, n_j$  the populations and  $g_i, g_j$  their corresponding statistical weights of levels  $i$  and  $j$ ), we set  $\frac{dV}{dr}$  as:

$$\left( \frac{dV}{dr} \right)_{\text{VIR}} = 0.65\sqrt{\alpha} \left[ \frac{n_{\text{H}}}{10^3 \text{ cm}^{-3}} \right]^{1/2} \text{ km s}^{-1} \text{ pc}^{-1}, \quad (\text{A2})$$

suitable for a mostly self-gravitating gas phase (Papadopoulos & Seaquist 1999), where  $\alpha$  depends on the assumed density profile and  $n_{\text{H}}$  is the total H-nucleus density. This ensures that the optical depth of the transition  $ij$  is a local quantity everywhere within the cloud, as expected for macroturbulent velocity fields. For this work we adopt  $0.65\sqrt{\alpha} = 1$ .

## REFERENCES

- Asplund, M., Grevesse, N., Sauval, A. J., & Scott, P. 2009, *ARA&A*, 47, 481
- Bialy, S., & Sternberg, A. 2014, arXiv:1409.6724
- Bayet, E., Williams, D. A., Hartquist, T. W., & Viti, S. 2011, *MNRAS*, 414, 1583
- Bell, T. A., Roueff, E., Viti, S., & Williams, D. A. 2006a, *MNRAS*, 371, 1865

- Bell, T. A., Hartquist, T. W., Viti, S., & Williams, D. A. 2006b, *A&A*, 459, 805
- Bergin, E. A., & Tafalla, M. 2007, *ARA&A*, 45, 339
- Bisbas, T. G., Bell, T. A., Viti, S., Yates, J., & Barlow, M. J. 2012, *MNRAS*, 427, 2100
- Bisbas, T. G., Bell, T. A., Viti, S., et al. 2014, *MNRAS*, 443, 111
- Bolatto, A. D., Jackson, J. M., & Ingalls, J. G. 1999, *ApJ*, 513, 275
- Bolatto, A. D., Wolfire, M., & Leroy, A. K. 2013, *ARA&A*, 51, 207
- Bryant, P. M., & Scoville, N. Z. 1996, *ApJ*, 457, 678
- Christensen, C., Quinn, T., Governato, F., et al. 2012, *MNRAS*, 425, 3058
- Cronin, N. J., Gillespie, A. R., Huggins, P. J., & Phillips, T. G. 1976, *A&A*, 46, 135
- Daddi, E., Dannerbauer, H., Liu, D., et al. 2014, arXiv:1409.8158
- Daddi, E., Bournaud, F., Walter, F., et al. 2010, *ApJ*, 713, 686
- Devereux, N., Taniguchi, Y., Sanders, D. B., Nakai, N., & Young, J. S. 1994, *AJ*, 107, 2006
- Dickman, R. L., Snell, R. L., & Schloerb, F. P. 1986, *ApJ*, 309, 326
- Downes, D., & Solomon, P. M. 1998, *ApJ*, 507, 615
- Draine, B. T. 1978, *ApJS*, 36, 595
- Dumke, M., Nieten, C., Thuma, G., Wielebinski, R., & Walsh, W. 2001, *A&A*, 373, 853
- Gaches, B. A. L., Offner, S. S. R., Rosolowsky, E. W., & Bisbas, T. G. 2014, arXiv:1412.2754
- Gao, Y., & Solomon, P. M. 2004, *ApJS*, 152, 63
- Glover, S. C. O., Clark, P. C., Micic, M., & Molina, F. 2014, arXiv:1403.3530
- Graciá-Carpio, J., García-Burillo, S., Planesas, P., & Colina, L. 2006, *ApJ*, 640, L135
- Graciá-Carpio, J., García-Burillo, S., Planesas, P., Fuente, A., & Usero, A. 2008, *A&A*, 479, 703
- Greve, T. R., Papadopoulos, P. P., Gao, Y., & Radford, S. J. E. 2009, *ApJ*, 692, 1432
- Guesten, R., Serabyn, E., Kasemann, C., et al. 1993, *ApJ*, 402, 537

- Hodge, J. A., Carilli, C. L., Walter, F., et al. 2012, *ApJ*, 760, 11
- Hollenbach, D. J., & Tielens, A. G. G. M. 1999, *Reviews of Modern Physics*, 71, 173
- Hughes, D. H., Serjeant, S., Dunlop, J., et al. 1998, *Nature*, 394, 241
- Hughes, A., Wong, T., Ott, J., et al. 2010, *MNRAS*, 406, 2065
- Israel, F. P. 1997, *A&A*, 328, 471
- Iverson, R. J., Smail, I., Papadopoulos, P. P., et al. 2010, *MNRAS*, 404, 198
- Krips, M., Neri, R., García-Burillo, S., et al. 2008, *ApJ*, 677, 262
- McElroy, D., Walsh, C., Markwick, A. J., et al. 2013, *A&A*, 550, A36
- Lagos, C. d. P., Bayet, E., Baugh, C. M., et al. 2012, *MNRAS*, 426, 2142
- Larson, R. B. 1981, *MNRAS*, 194, 809
- Leech, J., Isaak, K. G., Papadopoulos, P. P., Gao, Y., & Davis, G. R. 2010, *MNRAS*, 406, 1364
- Madden, S. C., Poglitsch, A., Geis, N., Stacey, G. J., & Townes, C. H. 1997, *ApJ*, 483, 200
- Maloney, P., & Black, J. H. 1988, *ApJ*, 325, 389
- Mao, R.-Q., Schulz, A., Henkel, C., et al. 2010, *ApJ*, 724, 1336
- Meijerink, R., Spaans, M., Loenen, A. F., & van der Werf, P. P. 2011, *A&A*, 525, AA119
- Millar, T. J., Farquhar, P. R. A., & Willacy, K. 1997, *A&AS*, 121, 139
- Narayanan, D., Krumholz, M., Ostriker, E. C., & Hernquist, L. 2011, *MNRAS*, 418, 664
- Nguyen, Q.-R., Jackson, J. M., Henkel, C., Truong, B., & Mauersberger, R. 1992, *ApJ*, 399, 521
- Offner, S. S. R., Bisbas, T. G., Viti, S., & Bell, T. A. 2013, *ApJ*, 770, 49
- Offner, S. S. R., Bisbas, T. G., Bell, T. A., & Viti, S. 2014, *MNRAS*, 440, L81
- Padoan, P., & Nordlund, Å. 2002, *ApJ*, 576, 870
- Paglione, T. A. D., Jackson, J. M., & Ishizuki, S. 1997, *ApJ*, 484, 656

- Pak, S., Jaffe, D. T., van Dishoeck, E. F., Johansson, L. E. B., & Booth, R. S. 1998, *ApJ*, 498, 735
- Papadopoulos, P. P., & Seaquist, E. R. 1999, *ApJ*, 516, 114
- Papadopoulos, P. P., Thi, W.-F., & Viti, S. 2002, *ApJ*, 579, 270
- , 2004, *MNRAS*, 351, 147
- Papadopoulos, P. P. 2007, *ApJ*, 656, 792
- Papadopoulos, P. P., Isaak, K. G., & van der Werf, P. P. 2007, *ApJ*, 668, 815
- Papadopoulos, P. P. 2010a, *ApJ*, 720, 226
- Papadopoulos, P. P., van der Werf, P., Isaak, K., & Xilouris, E. M. 2010b, *ApJ*, 715, 775
- Papadopoulos, P. P., van der Werf, P. P., Xilouris, E. M., et al. 2012a, *MNRAS*, 426, 2601
- Papadopoulos, P. P., van der Werf, P., Xilouris, E., Isaak, K. G., & Gao, Y. 2012b, *ApJ*, 751, 10
- Papadopoulos, P. P., Zhang, Z.-Y., Xilouris, E. M., et al. 2014, *ApJ*, 788, 153
- Pelupessy, F. I., Papadopoulos, P. P., & van der Werf, P. 2006, *ApJ*, 645, 1024
- Pelupessy, F. I., & Papadopoulos, P. P. 2009, *ApJ*, 707, 954
- Riechers, D. A., Hodge, J., Walter, F., Carilli, C. L., & Bertoldi, F. 2011, *ApJ*, 739, LL31
- Smail, I., Ivison, R. J., & Blain, A. W. 1997, *ApJ*, 490, L5
- Solomon, P. M., Downes, D., & Radford, S. J. E. 1992, *ApJ*, 387, L55
- Solomon, P. M., Downes, D., Radford, S. J. E., & Barrett, J. W. 1997, *ApJ*, 478, 144
- Tomassetti, M., Porciani, C., Romano-Díaz, E., Ludlow, A. D., & Papadopoulos, P. P. 2014, *MNRAS*, 445, L124
- van Dishoeck, E. F. 1998, *The Molecular Astrophysics of Stars and Galaxies*, edited by Thomas W. Hartquist and David A. Williams. Clarendon Press, Oxford, 1998., p.53, 4, 53
- Vazquez-Semadeni, E. 1994, *ApJ*, 423, 681

- Walch, S. K., Whitworth, A. P., Bisbas, T., Wünsch, R., & Hubber, D. 2012, MNRAS, 427, 625
- Wilson, R. W., Jefferts, K. B., & Penzias, A. A. 1970, ApJ, 161, L43
- Wolfire, M. G., Hollenbach, D., & McKee, C. F. 2010, ApJ, 716, 1191
- Xie, T., Allen, M., & Langer, W. D. 1995, ApJ, 440, 674
- Yao, L., Seaquist, E. R., Kuno, N., & Dunne, L. 2003, ApJ, 588, 771 (2003a)
- Yao, L., Seaquist, E. R., Kuno, N., & Dunne, L. 2003, ApJ, 597, 1271 (2003b)
- Young, J. S., & Scoville, N. Z. 1991, ARA&A, 29, 581
- Zhang, Z.-Y., Gao, Y., Henkel, C., et al. 2014, ApJ, 784, LL31